ELSEVIER

Biophysical Chemistry 126 (2007) 209–217

Biophysical Chemistry

http://www.elsevier.com/locate/biophyschem

Compartmentalization of the Type I Fcε receptor and MAFA on mast cell membranes

B. George Barisas [a,*], Steven M. Smith [b], Jingjing Liu [b], Jinming Song [a], Guy M. Hagen [a], Israel Pecht [c], Deborah A. Roess [b]

[a] *Department of Chemistry, Colorado State University, Fort Collins, CO 80523, USA*
[b] *Department of Biomedical Sciences, Colorado State University, Fort Collins, CO, USA*
[c] *Department of Immunology, The Weizmann Institute of Science, Rehovot, Israel*

Received 5 May 2006; accepted 17 May 2006
Available online 21 June 2006

Abstract

The Mast cell Function-associated Antigen (MAFA) is a membrane glycoprotein on rat mast cells (RBL-2H3) expressed at a ratio of ~1:30 with respect to the Type I Fcε receptor (FcεRI). Despite this stoichiometry, clustering MAFA by its specific mAb G63 substantially inhibits secretion of both granular and de novo synthesized mediators induced upon FcεRI aggregation. Since the FcεRIs apparently signal from within raft micro-environments, we investigated possible co-localization of MAFA within these membrane compartments containing aggregated FcεRI. We used cholera toxin B subunit (CTB) to cluster the raft component ganglioside GM1 and studied the effects of this perturbation on rotation of FcεRI and MAFA by time-resolved phosphorescence anisotropy of erythrosin-conjugated probes. CTB treatment would be expected to substantially inhibit rotation of raft-associated molecules. Experimentally, CTB has no effect on rotational parameters such as the long-time anisotropy (r_∞) of unperturbed FcεRI or MAFA. However, on cells where FcεRI-IgE has previously been clustered by antigen (DNP_{14}-BSA), CTB treatment increases the FcεRI-IgE's r_∞ by 0.010 and MAFA's by 0.014. Similarly, CTB treatment of cells where MAFA had been clustered by mAb G63 increases MAFA's r_∞ by 0.010 but leaves FcεRI's unaffected. Evaluation of raft localization of FcεRI and MAFA using sucrose gradient ultracentrifugation of Triton X-100 treated membrane fragments demonstrates that a significant fraction of MAFA molecules sediments with rafts when FcεRI is clustered by antigen or when MAFA itself is clustered by mAb G63. The large excess of FcεRI over MAFA explains why clustering MAFA does not substantively affect FcεRI dynamics. Moreover, in single-particle tracking studies of individual FcεRI-IgE or MAFA molecules, these proteins, upon clustering by antigen, move into small membrane compartments of reduced, but similar, dimensions. This provides additional indication of constitutive interactions between FcεRI and MAFA. Taken together, these results of distinct methodologies suggest that MAFA functions within raft microdomains of the RBL-2H3 cell membrane and thus in close proximity to the FcεRI which themselves signal from within the raft environment.

Keywords: FcεRI; MAFA; 2H3; Plasma membrane rafts; Signaling; Single-particle tracking

1. Introduction

The Type I Fcε receptors expressed on mast cells and basophils (FcεRI) are specific for the respective Fcε domains of IgE molecules and bind them with a stoichiometry of 1:1. Although binding by itself does not the initiate secretory response of these cells, clustering of the FcεRI via the bound IgEs which serve as antigen-specific, divalent adaptors provide the signal leading to the above cellular response [1]. This response involves secretion of both granule-stored mediators

Abbreviations: 2H3, rat mucosal-type mast cells of the 2H3 cell line; BSS, balanced salt solution; CTB, cholera toxin B subunit; *D*, diffusion coefficient; DMEM, Dulbecco's Modified Eagle's Medium; DNP, 2,4-dinitrophenyl; Er, erythrosin isothiocyanate; FcεRI, Type I Fcε receptor; FPR (or FRAP), fluorescence photobleaching recovery; GPI, glycosylphosphatidyl-inositol; ITIM, immuno-receptor tyrosine-based inhibitory motif; M, fractional mobility; mAb, monoclonal antibody; MAFA, mast cell function-associated antigen; MEM, minimal essential medium; PTK, protein tyrosine kinase.

* Corresponding author. Tel.: +1 970 491 6641; fax: +1 970 491 1801.
E-mail address: barisas@lamar.colostate.edu (B.G. Barisas).

0301-4622/$ - see front matter © 2006 Elsevier B.V. All rights reserved.
doi:10.1016/j.bpc.2006.05.026

such as histamine as well as the de novo synthesized ones [2] utilizing a signaling network that includes recruitment and activation of specific protein tyrosine kinases (PTK) [3], a transient increase in tyrosine phosphorylation of several cellular proteins [4,5] and free intracellular calcium ion concentrations [6] and activation of PLCγ and phosphatidyl inositide hydrolysis [7].

Several membrane proteins, including a membrane glycoprotein termed the Mast cell Function-associated Antigen (MAFA), have been found to suppress the FcεRI-mediated secretory response [8–12] upon being clustered by the specific mAb G63. Although there is only approximately one MAFA expressed for every thirty FcεRI, clustering MAFA was shown to inhibit by up to 80% the secretory response of the rat mucosal-type mast cells of the RBL-2H3 line to subsequent FcεRI clustering [13]. MAFA apparently delivers negative signals overriding those of the aggregated FcεRI upstream of PLCγ activation by suppressing both phosphatidylinositide phosphate hydrolysis and transient intracellular calcium elevation [13,14] and these inhibitory effects are not due to MAFA interference with IgE-FcεRI interactions [13]. Pecht et al. have shown that MAFA clustering induces phosphorylation of the tyrosine residue of its immuno-receptor tyrosine-based inhibitory motif (ITIM) by the PTK *lyn* [15] . This induces recruitment to this ITIM of both SHIP, presumably causing reduction of PIP3 levels [15], and SHP2, lowering *syk* activity [16].

Previous studies suggest functionally significant interactions between FcεRI and MAFA within the cell membrane. Fluorescence resonance energy transfer measurements demonstrate proximity of FcεRI to MAFA binding mAb G63 [17]. Time-resolved phosphorescence anisotropy measurements of rotational dynamics of FcεRI and MAFA [18] suggest that these molecules are constitutively associated with one another, at least to some extent, irrespective of MAFA's aggregation state. Thus, it is important to determine whether these interactions occur at arbitrary sites in the plasma membrane or in well-defined membrane compartments. Membrane microdomains include so-called rafts which, because of their high cholesterol and sphingolipid content, float in sucrose gradients. Rafts are enriched, not only with sphingolipids and cholesterol [19], but also with glycosylphosphatidyl-inositol (GPI)-anchored proteins [20] and, in some cells, comprise a substantial fraction of the plasma membrane [21,22]. These microdomains can contain membrane proteins necessary for cell signaling [23,24] and have been reported to diffuse laterally as intact entities within the plasma membrane [25]. Baird's group has shown that unperturbed, non-aggregated FcεRI are dispersed within the plasma membrane but, upon aggregation, are translocated into lipid rafts [26]. To independently examine the effects of FcεRI clustering on the compartmentalization of MAFA or FcεRI, we have now combined several methods, time-resolved phosphorescence anisotropy measurements of protein rotation, density gradient ultracentrifugation and single-particle tracking of individual protein molecules on viable cells in order to evaluate the characteristics of membrane compartments accessed by MAFA and FcεRI.

2. Materials and methods

2.1. Cells and culture

Rat mucosal-type mast cells of the RBL-2H3 line were kindly provided by Dr. Reuben Siraganian of the National Institutes of Health. Cells were grown and characterized as described [18] in Minimum Essential Medium Eagle with Earle's salts (VWR), containing HEPES buffer and non-essential amino acids (Sigma-Aldrich, St. Louis, MO) and supplemented with 10% fetal bovine serum (Gemini Bio Products, Woodland, CA). Cells were grown to approximately 90% confluence in BD Falcon non-treated, plug-seal tissue culture flasks (VWR), which they prefer, and then seeded into Petri dishes for high-throughput cell culture. For raft experiments, 20 dishes were usually grown to provide the necessary 25 million cells per sample. Cells were harvested from culture using a 5 mM EDTA in PBS for 10 min at 4 °C and then washed down using Hank's Balanced Salt Solution.

2.2. Antibodies, proteins and conjugates

mAb G63 (IgG_1) was purified from hybridoma culture supernatants by chromatography [18]. Monoclonal 2-4-dinitrophenyl (DNP)-specific A2 mouse IgE was purified from ascitic fluid by binding to DNP-Sepharose and elution with DNP-glycine [13]. FcεRI alpha chain-specific antibody was obtained from Upstate Cell Signaling Solutions, Lake Placid, NY. DNP_{14}-BSA, derivatized with an average of 14 DNP-groups per molecule, was prepared as described earlier [27]. Antibodies were derivatized with erythrosin isothiocyanate (Er, Molecular Probes, Eugene, OR) using a modification [18] of methods described by Johnson and Holborow [28]. Prior to use, all dye-derivatized proteins were centrifuged at 130,000×*g* for 10 min in a Beckman Airfuge (Beckman Instruments, Palo Alto, CA) to remove any protein aggregates formed during storage.

2.3. Time-resolved phosphorescence anisotropy measurements

Time-resolved phosphorescence anisotropy (TPA) experiments were performed using methods previously described [29,30] as adapted for MAFA [18]. Cells were labeled either

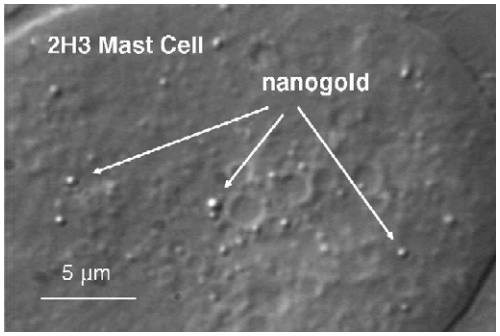

Fig. 1. Photograph of 2H3 cell showing IgE-nanogold particles bound to individual Type I Fcε receptors.

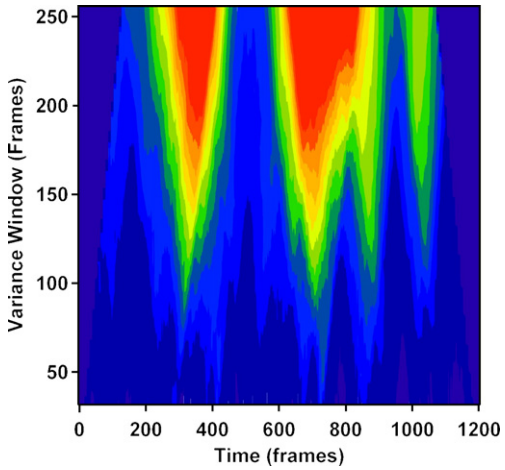

Fig. 2. 3D plot of normalized variance of IgE-binding gold nanoparticle position on a 2H3 cell within time windows of durations ranging from 256 frames (top) to 32 frames (bottom). Windows are translated along particle trajectory. Times of inter-domain jumps are indicated by peaks.

with erythrosin isothiocyanate (Er)-conjugated A2-IgE to monitor FcεRI or with Er-G63 Fab to monitor MAFA. Typical conditions were 150 nM and 30 nM, for FcεRI and MAFA, respectively, for 1 h at 4 °C. Phosphorescence from deoxygenated cell samples [31] was excited by 532 nm pulses from a Nd:YAG laser. Phosphorescence emitted polarized parallel $I_{\|}(t)$ and perpendicular $I_{\perp}(t)$ to the exciting light were analyzed to yield a phosphorescence intensity function $s(t)=I_{\|}(t)+2I_{\perp}(t)$ and a phosphorescence anisotropy function $r(t)=[I_{\|}(t)-I_{\perp}(t)]/s(t)$. Anisotropy data were analyzed according to a single average exponential decay model $r(t)=r_{\infty}+(r_0-r_{\infty})\exp(-t/\varphi)$ which yielded the initial anisotropy value r_0, the limiting anisotropy value r_{∞} and the rotational correlation time φ [18].

2.4. Density-gradient fractionation of RBl-2H3 cell membrane extracts

To isolate membrane rafts from RBL-2H3 cells, 5×10^7 cells were washed two times with Hank's Balanced Salt Solution, pH 7.2 (BSS) and then lysed for 5–10 min on ice in 1 ml of a buffer containing 25 mM MES, 150 mM NaCl, 2 mM EDTA, 0.25% Triton-X100, and protease inhibitors including aprotinin, leupeptin, EDTA, and PMSF (Roche). 1 mL of the cell lysate solution containing plasma membrane fragments was then combined with 1 mL of 80% sucrose to produce a 40% sucrose solution. A discontinuous sucrose gradient from 10% to 80% was created with the sample in 40% sucrose layered within this gradient. The gradient was loaded into a Beckman SW-41 swinging bucket rotor and spun at 175,000×g for 20 h at 4 °C. After the spin, eighteen 650 μL fractions were carefully collected from the top of the gradient downward. A 50 μL aliquot from each fraction was diluted 1:1 with 95% SDS and 5% β-mercaptoethanol. After separation of proteins from each fraction using SDS-PAGE and transfer of proteins to nitrocellulose, proteins of interest, MAFA and the FcεRI receptor were identified using 4–10 μg of the MAFA-specific antibody G63 or anti-FcεRI alpha chain antibody (Upstate Cell Signaling Solutions, Lake P lacid, NY), respectively. Blots were incubated 5 min with "Super Signal West Pico" chemiluminescence detection substrate (3 mL peroxide solution plus 3 mL luminol enhancer solution (Pierce-Endogen, Rockford, IL) and recorded by 1–5 min exposure on Amersham Enhanced ECL film (Amersham Pharmacia Biotech, England). The amount of MAFA or receptor in each fraction was measured using a Bio-Rad GS-800 calibrated densitometer. The sucrose concentration in each fraction was determined using a Bausch and Lomb refractometer. For all experiments, cells were pre-incubated with 100 ng/mL DNP-specific A2-IgE for 1 h at 37 °C prior to further treatment. FcεRI-IgE clustering was achieved in cells suspended in BSS by incubation with 100 nM of the antigen, DNP_{14}-BSA for 45 min at room temperature [32]. Aggregation of MAFA was accomplished by treating cells MAFA-specific mAb G63 in BSS for 1 h at 37 °C.

2.5. Single-particle tracking of FLAG-LHR-wt receptors on individual cells

Lateral dynamics and the size of domains accessed by individual FcεRI or MAFA were evaluated using single-particle tracking (SPT) methods as described by Kusumi et al. [33]. 40 nm gold particles (Ted Pella, Inc., Redding, CA) were conjugated with IgE or mAb G63 or its Fab fragments, essentially as described by Daumas et al. [34] who estimated an average of two antibody molecules bound per nanoparticle. RBL-2H3 cells grown on a coverslip were then incubated with 100 μL of antibody-conjugated nanogold at a concentration of 9×10^{10} particles/mL for 1 h at 4 °C. This labeling typically produced 1–4 gold particles per cell. Binding of these mAbs was specific for either FcεRI or MAFA as, when cells were preincubated with a 10-fold excess of antibody, no particles were detected on the cells (Fig. 1).

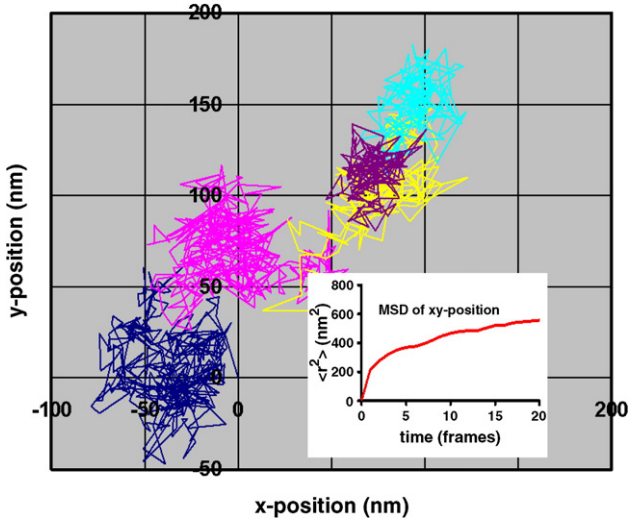

Fig. 3. Segmentation of trajectory of a IgE-binding gold nanoparticle on a 2H3 cell into domain regions by the method shown in Fig. 1. Analysis of the size of a domain and the particle residence time provides an estimate of the macroscopic diffusion coefficient expected for the receptors to which the particle attaches.

Table 1
Effects of cholera toxin treatment on the limiting rotational anisotropy of FcεRI and MAFA, with and without pre-crosslinking by DNP_{14}-BSA and anti-G63 Fab [a]

Protein aggregated initially [b]	Membrane species for which rotational limiting anisotropy (r_∞) measured subsequently					
	Er-IgE-FcεRI			Er-G63 Fab-MAFA		
	No CTB (control)	CTB-treated	r_∞ change caused by CTB	No CTB (control)	CTB-treated	r_∞ change caused by CTB
None	0.046	0.046	0	0.048	0.047	0
FcεRI	0.062	0.072	+0.010 [c]	0.047	0.061	+0.014 [c]
MAFA	0.059	0.057	0	0.051	0.061	+0.010 [c]

[a] The labeling sequence was (1) 150 nm unlabeled-IgE or Er-IgE at 4 °C for 1 h; (2) for measuring MAFA rotation and/or MAFA crosslinking, 30 nm Er-G63Fab or 30 nm unlabeled G63Fab, respectively, at 4 °C for 1 h; (3) FcεRI or MAFA crosslinking by treatment with 14 μg/ml DNP_{14}-BSA at 4 °C for 1 h or 4 μg/ml goat anti-mouse Fab at 37 °C for 1/2 h, respectively; and finally, (4) 5 μg/ml biotin–cholera toxin subunit B at 4 °C for 1 h followed by 4 μg/ml streptavidin at 37 °C for 5 min or comparable control incubation in buffer.

[b] All FcεRI were initially saturated with DNP-specific A2-IgE. When required, FcεRI were aggregated by treatment with DNP_{14}-BSA and MAFA was aggregated by treatment with monovalent G63 Fab fragments followed by goat anti-mouse Fab, respectively, as described above.

[c] Superscript indicates circumstances where CTB treatment produced a significant increase in the limiting rotational anisotropy of the membrane species probed.

Individual nanoparticles were imaged by differential interference contrast using a 63×1.4 NA oil immersion objective and a 1.4 NA oil condenser on a Zeiss Axiovert 135 microscope with a 2.5× Optovar and 2× C-mount adapter. Images were acquired using a Dage IFG-300 camera and were recorded for 2 min (3600 frames) at approximately 30 nm/pixel under the control of Metamorph software (Molecular Devices Corporation, Sunnyvale, CA). The trajectories for individual gold particles were segmented into compartments by calculation of statistical variance in particle position over times using a procedure similar to that developed by other investigators [34]. The normalized variance s_i^2 of a particle's position $(x_i y_i)$ at a particular frame time i within a window of duration n frames was calculated as

$$s_i^2 = \frac{n\sum_{j=i-n/2}^{i+n/2-1} x_j^2 - \left(\sum_{j=i-n/2}^{i+n/2-1} x_j\right)^2}{n^2(n-1)} + \frac{n\sum_{j=i-n/2}^{i+n/2-1} y_j^2 - \left(\sum_{j=i-n/2}^{i+n/2-1} y_j\right)^2}{n^2(n-1)}$$

Translating windows along the particle trajectory produced plots where peaks indicate inter-compartment jumps and multiple plots for a range of window durations can be presented as a 3-dimensional graph such as shown in Fig. 2. Such a graph allows individual inter-compartment jump times to be identified using whatever window length provides maximum information. The times of jumps thus identified were used to segment particle trajectories into discrete domains, such as shown in Fig. 3. Segmented trajectories were then analyzed to yield the domain sizes and residence times for each particle. Residence times were calculated as the time between jumps, while the compartment diagonal was estimated as $[12(s_x^2+s_y^2)]^{1/2}$ where s_x^2 and s_y^2 are the x- and y-variances of particle position within each domain. Effective macroscopic diffusion constants were calculated as the square of the compartment diagonal L_r divided by four times the residence time τ in the compartment as previously described [36]. Typically, 3–5 inter-compartment jumps were examined for each nanogold particle tracked.

3. Results and discussion

To explore possible MAFA-FcεRI interactions and their possible relation to MAFA's inhibition of secretion, we have previously studied by time-resolved phosphorescence anisotropy the rotational behavior of both MAFA and FcεRI in both unperturbed states and as ligated by various reagents involved in FcεRI-induced secretion and MAFA-mediated inhibition thereof [18,37]. From 4 °C to 37 °C the rotational correlation times of FcεRI-bound, erythrosin-conjugated IgE resemble those observed for MAFA-bound erythrosin-conjugated G63 Fab, 82±17 μs and 79±31 μs at 4 °C, respectively. Clustering the FcεRI-IgE complex by antigen or by anti-IgE increases the initial and limiting phosphorescence anisotropies of MAFA-bound erythrosin-conjugated G63 Fab and slows its rotational relaxation. Antigen clustering of the FcεRI-IgE complex has also been found to slow the lateral diffusion of cell-bound G63 Fab [18].

It has previously been demonstrated that clustering FcεRI causes the receptor to enter membrane raft microdomains [38]. The ganglioside GM1 characterizes these domains and its clustering increases the ordering of raft lipids. Thus, we induced extensive GM1 aggregation by treating cells with a CTB-biotin conjugate followed by addition of streptavidin and examined the impact of this aggregation on the rotation of FcεRI and MAFA. Key results of these experiments are summarized in Table 1 while a sample experimental trace is shown in Fig. 4. In

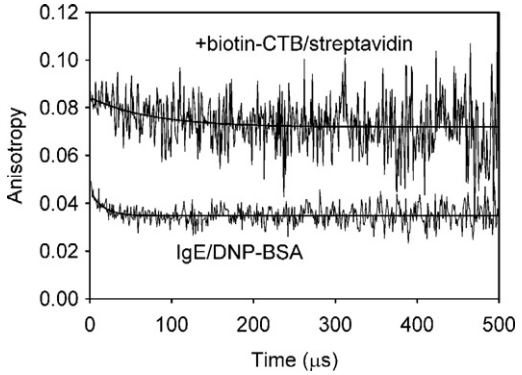

Fig. 4. Effect of CTB treatment on rotation of A2 IgE-binding FcεRI aggregated by DNP_{14}-BSA. Time-resolved phosphorescence anisotropy measurements of protein rotation were performed at 4 °C as described in the text. The increased limiting anisotropy induced by CTB suggests that the aggregated FcεRI are associated with raft microdomains.

this figure, the lower trace depicts anisotropy decay, and hence, rotation, of FcεRI binding phosphorescent Er-IgE and clustered by DNP_{14}-BSA. The upper trace shows anisotropy decay for a similar sample but additionally treated, before measurement, with CTB-biotin and streptavidin to aggregate GM1. This GM1 aggregation produces a substantial increase in limiting anisotropy r_∞ of the aggregated IgE-FcεRI, indicating that a considerable fraction of receptors has been rotationally immobilized. This is to be expected since, as described earlier, DNP-BSA aggregated receptors are known to translocate into lipid rafts where their mobility would be restricted by ordering of the raft lipid GM1. Table 1 summarizes the results of the entire series of such experiments. In each line, the entry in first column indicates which membrane molecule was aggregated prior to measurements included on that line of the table. The next three columns indicate, for FcεRI rotation on cells thus pretreated, the limiting anisotropies observed on otherwise untreated cells, on cells treated with biotin-CTB and streptavidin just prior to rotation measurements and the anisotropy difference resulting from CTB treatment. The last three columns indicate the same data for MAFA rotation. CTB treatment significantly increases r_∞ only for the FcεRI-IgE that have been pre-clustered by antigen as shown in column 4. However, preclustering either FcεRI by antigen treatment or MAFA by G63 Fab and second antibody increases MAFA's r_∞ as shown in column 7. This would be explained if MAFA is pre-associated with the receptor and hence enters rafts when either species is aggregated. By this argument, aggregating MAFA would also translocate some receptors into rafts. However, since there is only one MAFA for every 30 receptors, the fractional increase in the receptors' measured r_∞ would be undetectable. Thus, these rotational diffusion studies are consistent with the notion that both MAFA and FcεRI preferentially translocate into raft domains, upon being clustered.

Table 2
Fractions of MAFA and FcεRI in present in low- and high-density membrane fractions extracted from variously treated cells [a]

Treatment	Protein blotted	% protein in 10–34% sucrose [b]	% protein in 39–80% sucrose	Number replicate expts.
None	FcεRI	16±4	84±4	2
None	MAFA	4±1	96±1	2
mAb G63	FcεRI	18±5	82±5	4
mAb G63	MAFA	42±8	58±8	3
DNP_{14}-BSA	FcεRI	40±2	60±2	3
DNP_{14}-BSA	MAFA	40±7	60±7	3

[a] Western blots from variously treated cells, such as those shown in Fig. 4, were subjected to quantitative densitometry to determine the fractions of MAFA and FcεRI present in low-density (10–34% sucrose) and high-density (39–80% sucrose) membrane fractions.

[b] Proteins banding within range of sucrose densities are typically described as lipid raft-associated. The first three entries are nominally unperturbed molecular species while the last three entries are dimerized (mAb G63 treatment prior to MAFA blot) or highly aggregated (DNP_{14}-BSA treatment prior to FcεRI or MAFA blot). One-tailed *t*-tests indicate that FcεRI aggregation significantly ($p<0.01$) increases the fraction of both FcεRI (lines 5 *vs*. 1) and MAFA (lines 5 *vs*. 2) present in low-density (raft) fractions while MAFA aggregation significantly increases only MAFA in rafts (lines 4 *vs*. 2).

To explore raft localization of MAFA and FcεRI in more detail, we have isolated plasma membrane rafts from RBL-2H3 cells using reported standard methods and examined conditions under which both MAFA and FcεRI appear in these micro-

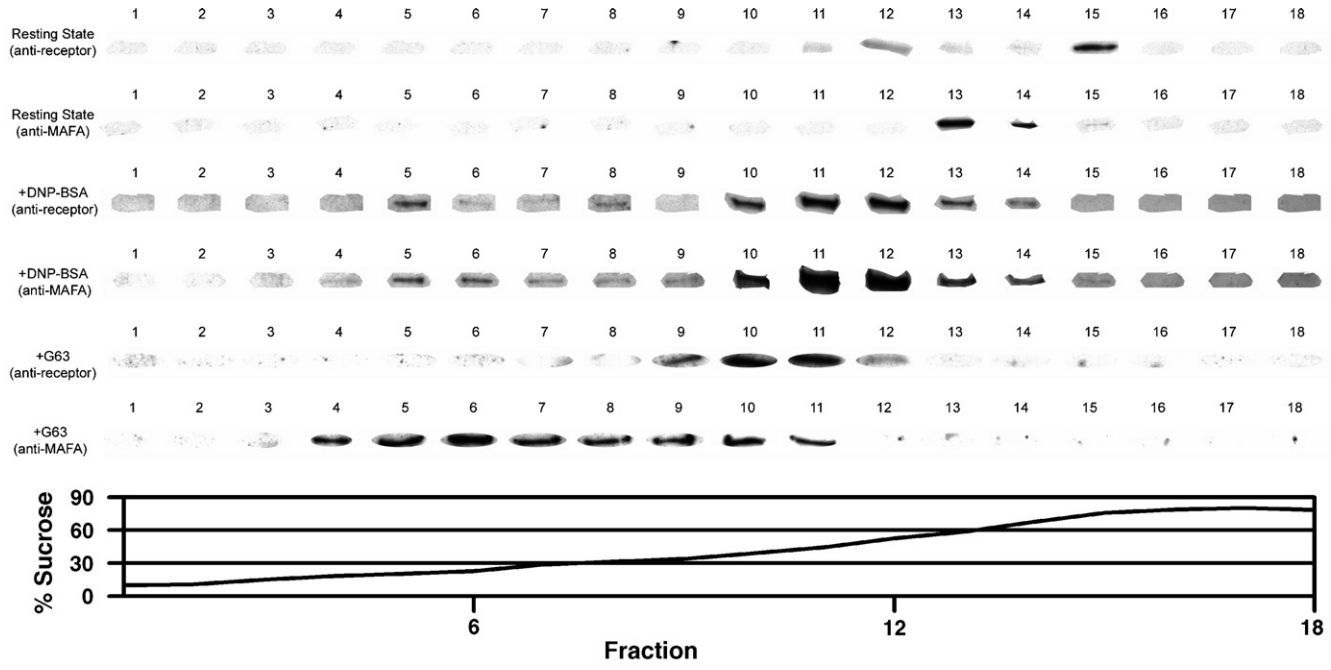

Fig. 5. Detection of aggregated MAFA and Fc,RI in low-density regions of sucrose gradients following ultracentrifugation of 2H3 cell membrane detergent extracts. Representative Western blots obtained demonstrate that FcεRI (panels 1, 3 and 5) is located in high-buoyancy membrane fractions only after crosslinking of receptor with DNP_{14}-BSA while MAFA (2, 4, and 6) moves into low-density membrane fractions after treatment of cells with either G63 antibody or crosslinking of FcεRI by DNP_{14}-BSA.

Table 3
Single-particle tracking of individual FcεRI or MAFA before and after crosslinking with DNP_{14}-BSA or G63 antibody

Pretreatment	Nanogold conjugate	Number of particles analyzed	D_{0-1} [a, b] (10^{-11} cm^2 s^{-1})	D_{hop} [a, c] (10^{-11} cm^2 s^{-1})	Residence time τ [a, d] (s)	Compartment diameter L_r [a, e] (nm)
None	IgE	25	1.1±0.7	0.30±0.12	22±16	163±87
DNP_{14}-BSA	IgE	27	0.5±0.4	0.03±0.05	24±14	53±53
G63	IgE	26	1.0±0.4	0.26±0.11	24±15	160±83
None	G63 Fab	13	5.8±1.4	0.42±0.12	16±9	164±67
None	G63 mAb	24	1.0±0.4	0.23±0.11	24±16	149±83
DNP_{14}-BSA	G63 mAb	26	0.9±0.1	0.09±0.02	23±12	90±31

[a] All uncertainties are presented as standard deviations (S.D.) of data sets, *not* as standard errors of means (S.E.M.).
[b] Diffusion coefficient within compartment calculated from first two points of MSD vs. time plot [34].
[c] Diffusion coefficient for hop diffusion between compartments as calculated from compartment size L and particle residence time τ as $L^2/4\tau$ [36].
[d] Average particle residence time within a compartment.
[e] The average diameter of an individual compartment calculated as described by Daumas et al. [34] and Murase et al. [35].

domains. Fig. 5 presents Western blots of FcεRI and MAFA in different sucrose fractions after density gradient fractionation of detergent extracts from variously-treated cells. As can be seen in the figure, there is a substantially larger amount of FcεRI in low buoyant density fractions, i.e., raft fractions, after clustering by antigen. Table 2 shows quantitative densitometric analysis of a number of such experiments. As was suggested by results of the rotation experiments described above, both DNP_{14}-BSA clustering of FcεRI-IgE and G63 clustering of MAFA cause substantially increased amounts of MAFA to appear in low-density plasma membrane fractions. Similarly, the amount of FcεRI found in membrane rafts is significantly increased upon FcεRI clustering with DNP_{14}-BSA, as shown previously by Baird et al. [38]. However, clustering MAFA with mAb G63 does not significantly increase the apparent amount FcεRI in raft fractions. This result is also consistent with constitutive MAFA interactions with the FcεRI receptor and with the known relative excess of FcεRI over MAFA. Thus, G63-clustered MAFA moves into rafts but, presumably each MAFA can bring only one FcεRI, or about 1/30 of the total available FcεRI, into these domains. One would not expect such a small change in the distribution FcεRI to be detectable in experiments such as these.

We then explored the lateral localization of individual MAFA and FcεRI molecules by means of single-particle tracking. IgE-nanogold, G63 Fab-nanogold and G63 mAb-nanogold probes were employed to examine the motions of FcεRI and MAFA, respectively. DNP_{14}-BSA treatment was used to cluster the receptors while intact mAb G63-nanogold probes presumably indicated motions of clustered MAFA. Calculation of the variance of particle position over various-sized time windows (Fig. 2) allowed segmentation of trajectory into individual compartments as shown in Fig. 3. The segmented trajectories were then analyzed to yield the diffusion coefficient D_{01} for mobility within each compartment, the residence time τ of particles in compartments, the compartment size L_r and the diffusion coefficient D_{hop} for hop diffusion between compartments. A summary of these results is shown in Table 3. On un-perturbed cells, the average compartment containing either FcεRI or MAFA was approximately 160 nm in diameter. However, specific clustering of either MAFA by G63 or FcεRI-IgE by DNP_{14}-BSA reduced the compartment size accessed by these molecules to 90 nm and 53 nm, respectively, though the residence time of receptors within these compartments remains essentially constant at about 20 s. The shift in the

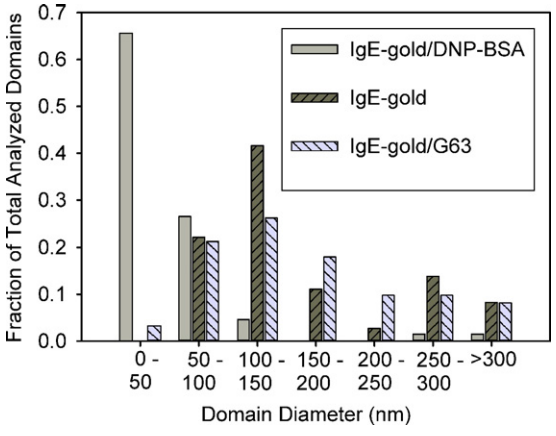

Fig. 6. Distribution of compartment sizes from single particle tracking of FcεRI. Individual values for compartment size calculated from particle tracks of FcεRI before and after crosslinking of FcεRI with DNP_{14}-BSA or crosslinking of MAFA with G63 antibody. Only DNP_{14}-BSA crosslinking moved FcεRI into smaller membrane compartments with 88% of receptors appearing in compartments with diameters of less than 75 nm.

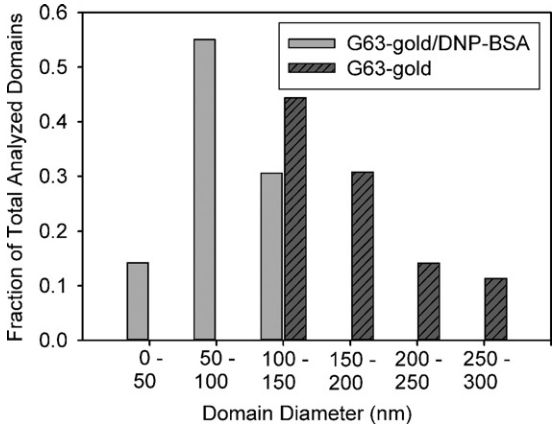

Fig. 7. Distribution of values for compartment size from single particle tracking of MAFA. Individual values for compartment sizes were calculated from particle tracks of MAFA before and after crosslinking of FcεRI with DNP_{14}-BSA.

Table 4
Combined effects of CTB and DNP_{14}-BSA pretreatments on SPT measurements of FcεRI and MAFA dynamics

Pretreatment	Nanogold conjugate	Number of particles analyzed	D_{0-1} [a, b] (10^{-11}cm^{2}s^{-1})	D_{hop} [a, c] (10^{-11} cm^2 s^{-1})	Residence time τ [a, d] (s)	Compartment diameter L [a, e] (nm)
CTB	IgE	10	3.0±2.4	0.38±0.17	29±16	210±104
CTB, DNP_{14}-BSA	IgE	10	2.1±1.2	0.21±0.06	33±21	167±69
CTB	G63	10	1.9±0.8	0.20±0.01	33±17	162±27
CTB, DNP_{14}-BSA	G63	10	2.6±2.0	0.32±0.20	34±17	209±115

[a] All uncertainties are presented as standard deviations (S.D.) of data sets, *not* as standard errors of means (S.E.M.).
[b] Diffusion coefficient within compartment calculated from first two points of MSD vs. time plot [34].
[c] Diffusion coefficient for hop diffusion between compartments as calculated from compartment size L and particle residence time τ as $L^2/4\tau$ [36].
[d] Average particle residence time within a compartment.
[e] The average diameter of an individual compartment calculated as described by Daumas et al. [34] and Murase et al. [35].

distribution of compartment sizes from large to small upon receptor clustering is more clearly depicted in Figs. 6 and 7 which show histograms of compartment sizes exhibited by FcεRI and MAFA on variously treated cells, respectively.

In a separate set of experiments, we examined the effects of CTB pre-treatment on single-particle dynamics of the FcεRI and MAFA under conditions analogous to those used for measuring FcεRI and MAFA rotation as discussed above. Cells were pre-treated with CTB (5 μg/ml for 50 min at 4 °C), bound with IgE- or G63-nanogold (50 min at 4 °C) and finally treated with antigen or buffer 14 (40 min at 4 °C). Results of these experiments are shown in Table 4. These results suggest that CTB pre-treatment hinders the antigen-induced movement of both FcεRI and MAFA into smaller membrane compartments since DNP_{14}-BSA treatment does not significantly reduce the compartment size accessed by either receptor. This would be expected if CTB binding to GM1 substantially increases raft lipid ordering which might, in turn, slow or restrict subsequent entry of aggregated FcεRI or MAFA into rafts. These molecules would then retain greater freedom from corralling by sub-membrane structures and so continue to access that same large compartments as before aggregation.

Results of the preceding SPT experiments raise the question of how the large and relatively stable compartments accessed by the receptors in these experiments may relate to possible localization of receptors in raft microdomains. While various estimates of raft size have earlier been put forward, recent high-speed single-particle tracking studies by Kusumi [35] suggest that 30–230 nm transient confinement zones observed for membrane lipids, with residence times of 1–17 ms, may be equated with rafts. However, the large compartments observed on much slower timescales, such as in the present study, must reflect different cell membrane structures. We have noted previously that, for various membrane species on the same cell, the residence time of these proteins in compartments tends to be relatively constant [39,40]. This would be the case if different dynamic structures, perhaps a cytoskeletal network, beneath the plasma membrane restricted or "corralled" membrane receptors for much of the time but fluctuated from time to time in their stability or in their association with the plasma membrane and so allowed membrane-resident molecules to escape. Raft microdomains would be expected to involve substantial concentration of signaling-related molecules such as kinases at the cytoplasmic face of the membrane. Thus, raft-associated species, such as FcεRI and MAFA after antigen clustering, might well prove more susceptible to compartmentalization by cytoskeletal structures than corresponding molecules in the bulk membrane and thus exhibit smaller average compartment sizes.

A key question concerning MAFA action is how is the relatively small number of MAFA molecules capable of such effective inhibition of cellular responses to FcεRI signaling. Several lines of work have indicated that MAFA is, to some extent, constitutively pre-associated with FcεRI on unperturbed 2H3 cells [17,37,41]. Moreover, co-clustering FcεRI and MAFA using bispecific reagents has been shown to provide more effective inhibition than MAFA clustering alone [42,43]. *Lyn* phosphorylation of MAFA's ITIM provides the site for recruitment and activation of the inhibitory phosphatase SHIP which depletes PLCγ reaction substrate [15] and for the protein tyrosine phosphatase SHP2 [16]. Since FcεRI signaling derives from receptor ITAM-specific phosphorylation in rafts by *lyn*, raft-associated receptors should provide sites of increased *lyn* concentration. Both because *lyn* activity is highest within lipid rafts and because of the presumed small dimensions of rafts, any translocation of MAFA into rafts could cause an enhanced inhibitory effect. Moreover, MAFA co-aggregated with FcεRI might encounter an even higher local concentration of *lyn* than separately clustered MAFA. This would amplify the inhibitory process by having *lyn* produce additional phosphorylation of the MAFA ITIM and the increase subsequent recruitment and activation of SHIP. Further, recent studies have shown that FcεRI phosphorylation reflects a dynamic balance between intrinsic *lyn* activity and FcεRI dephosphorylation by phosphatases such as SHP-1 [44]. Thus, MAFA co-aggregated with the receptor might additionally contribute to reduced steady-state receptor phosphorylation.

Acknowledgments

This work was supported in part by grants from NSF (DBI-0138322 and MCB-0315798) and NIH (HD23236).

References

[1] C. DeLisi, The biophysics of ligand–receptor interactions, Quarterly Reviews of Biophysics 13 (1980) 201–230.

[2] L. Schwartz, Mast cells: function and contents, Current Opinions in Immunology 6 (1994) 91–97.
[3] E. Eiseman, J.B. Bolen, Engagement of the high affinity IgE receptor activates SRC protein related tyrosine kinases, Nature 355 (1992) 78–80.
[4] A.M. Scharenberg, S. Lin, B. Cuenod, H. Yamamura, J. Kinet, Reconstitution of interactions between tyrosine kinases and the high affinity IgE receptor which are controlled by receptor clustering, The EMBO Journal 14 (1995) 3385–3394.
[5] M. Benhamou, J.S. Gutkind, K.C. Robbins, R.P. Siraganian, Tyrosine phosphorylation coupled to IgE receptor-mediated signal transduction and histamine release, Proceedings of the National Academy of Sciences of the United States of America 87 (1990) 5327–5330.
[6] R. Sagi-Eisenberg, H. Lieman, I. Pecht, Protein kinase C regulation of the receptor-coupled calcium signal in histamine-secreting rat basophilic leukaemia cells, Nature 313 (1985) 59–60.
[7] M. Beaven, J. Moore, G. Smith, T. Hesketh, J. Metcalfe, The calcium signal and phosphatidylinositol breakdown in 2H3 cells, Journal of Biological Chemistry 259 (1984) 7137–7142.
[8] N. Guo, G. Her, V. Reinhold, M. Brennan, R. Siraganian, V. Ginsburg, Monoclonal antibody AA4, which inhibits binding of IgE to high affinity receptors on rat basophilic leukemia cells, binds to novel α-galactosyl derivatives of ganglioside G_{D1b}, Journal of Biological Chemistry 264 (1989) 13267–13272.
[9] E. Ortega, A. Licht, Y. Biener, I. Pecht, A glycolipid-specific monoclonal antibody modulates Fcϵ, receptor stimulation of mast cells, Molecular Immunology 27 (1990) 1269–1277.
[10] V. Stephan, N. Guo, V. Ginsburg, R. Siraganian, Immunoprecipitation of membrane proteins from rat basophilic leukemia cells by the antiganglioside monoclonal antibody AA4, The Journal of Immunology 146 (1991) 4271–4277.
[11] S. Kitani, E. Berenstein, S. Mergenhagen, P. Tempst, R. Siraganian, A cell surface glycoprotein of rat basophilic leukemia cells close to the high affinity IgE receptor (FcγRI), Journal of Biological Chemistry 266 (1991) 1903–1909.
[12] M. Hamawy, C. Oliver, R. Siriganian, Inhibition of IgE binding to RBL-2H3 cells by a monoclonal antibody (BD6) to a surface protein other than the high affinity IgE receptor, The Journal of Immunology 148 (1992) 524–531.
[13] E. Ortega, I. Pecht, A monoclonal antibody that inhibits secretion from rat basophilic leukemia cells and binds to a novel membrane component, The Journal of Immunology 141 (1988) 4324–4332.
[14] M.D. Guthmann, M. Tal, I. Pecht, A new member of the C-type lectin family is a modulator of the mast cell secretory response, International Archives of Allergy and Immunology 107 (1995) 82–86.
[15] R. Xu, J. Abramson, M. Fridkin, I. Pecht, SH2 domain-containing inositol polyphosphate 5′-phosphatase is the main mediator of the inhibitory action of the mast cell function-associated antigen, Journal of Immunology 167 (2001) 6394–6402.
[16] R. Xu, I. Pecht, The protein tyrosine kinase syk activity is reduced by clustering the mast cell function-associated antigen, European Journal of Immunology 31 (2001) 1571–1581.
[17] L. Jurgens, D. Arndt-Jovin, I. Pecht, T.M. Jovin, Proximity relationships between the type I receptor for Fc epsilon (Fc epsilon RI) and the mast cell function-associated antigen (MAFA) studied by donor photobleaching fluorescence resonance energy transfer microscopy, European Journal of Immunology 26 (1996) 84–91.
[18] J. Song, G.M. Hagen, D.A. Roess, I. Pecht, B.G. Barisas, The mast cell function-associated antigen and its interactions with the type I Fcepsilon receptor, Biochemistry 41 (2002) 881–889.
[19] D.A. Brown, E. London, Structure and origin of ordered lipid domains in biological membranes, Journal of Membrane Biology 164 (1998) 103–114.
[20] S. Ilangumaran, D.C. Hoessli, Effects of cholesterol depletion by cyclodextrin on the sphingolipid microdomains of the plasma membrane, Biochemistry Journal 335 (1998) 433–440.
[21] F.R. Maxfield, Plasma membrane microdomains, Current Opinion in Cell Biology 14 (2002) 483–487.
[22] A. Gidwani, D. Holowka, B. Baird, Fluorescence anisotropy measurements of lipid order in plasma membranes and lipid rafts from RBL-2H3 mast cells, Biochemistry 40 (2001) 12422–12429.
[23] T. Harder, K. Simons, Caveolae, DIGs, and the dynamics of sphingolipid–cholesterol microdomains, Current Opinion in Cell Biology 9 (4) (1997) 534–542.
[24] Z. Xiao, P.N. Devreotes, Identification of detergent-resistant plasma membrane microdomains in dictyostelium: enrichment of signal transduction proteins, Molecular Biology of the Cell 8 (1997) 855–869.
[25] A. Pralle, P. Keller, E. Florin, K. Simons, J.K.H. Hörber, Sphingolipid–cholesterol rafts diffuse as small entities in the plasma membrane of mammalian cells, Journal of Cell Biology 148 (2000) 997–1008.
[26] K.A. Field, D. Holowka, B. Baird, Fc-epsilon-RI-mediated recruitment of p53/56lyn to detergent-resistant membrane domains accompanies cellular signaling, Proceedings of the National Academy of Sciences of the United States of America 92 (1995) 9201–9205.
[27] M.E. Carsten, H.N. Eisen, The interaction of dinitrobenzene derivatives with bovine serum albumin, Journal of the American Chemical Society 75 (1953) 4451–4456.
[28] G.D. Johnson, E.J. Holborow, Preparation and use of fluorochrome conjugates, in: D.M. Weir (Ed.), Handbook of Experimental Immunology, Blackwell Scientific Publications, Boston, 1986, p. 28.21.
[29] C.J. Philpott, N.A. Rahman, N. Kenny, B.G. Barisas, D.A. Roess, Rotational dynamics of luteinizing hormone receptors on bovine and ovine luteal cell plasma membranes, Biology of Reproduction 53 (1995) 645–650.
[30] B.G. Barisas, W.F. Wade, T.M. Jovin, D. Arndt-Jovin, D.A. Roess, Dynamics of molecules involved in antigen presentation: effects of fixation, Molecular Immunology 36 (1999) 701–708.
[31] P. Johnson, P.B. Garland, Depolarization of fluorescence depletion. A microscopic method for measuring rotational diffusion of membrane proteins on the surface of a single cell, FEBS Letters 132 (1981) 252–256.
[32] E.D. Sheets, D. Holowka, B. Baird, Critical role for cholesterol in Lyn-mediated tyrosine phosphorylation of FcεRI and their association with detergent-resistant membranes, Journal of Cell Biology 145 (1999) 877–887.
[33] C. Dietrich, B. Yang, T. Fujiwara, A. Kusumi, K. Jacobson, Relationship of lipid rafts to transient confinement zones detected by single particle tracking, Biophysical Journal 82 (2002) 274–284.
[34] F. Daumas, N. Destainville, C. Millot, A. Lopez, D. Dean, L. Salomé, Confined diffusion without fences of a G protein coupled receptor as revealed by single particle tracking, The Biophysical Journal 84 (2003) 356–366.
[35] K. Murase, T. Fujiwara, Y. Umemura, K. Suzuki, R. Iino, H. Yamashita, M. Saito, H. Murakoshi, K. Ritchie, A. Kusumi, Ultrafine membrane compartments for molecular diffusion as revealed by single molecule techniques, Biophysical Journal 86 (2004) 4075–4093.
[36] M.J. Saxton, Single-particle tracking: the distribution of diffusion coefficients, Biophysical Journal 72 (1997) 1744–1753.
[37] J. Song, G. Hagen, S.M. Smith, D.A. Roess, I. Pecht, B.G. Barisas, Interactions of the mast cell function-associated antigen with the type I Fcepsilon receptor, Molecular Immunology 38 (2002) 1315–1321.
[38] K.A. Field, D. Holowka, B. Baird, Structural aspects of the association of FcεRI with detergent-resistant membranes, Journal of Biological Chemistry 274 (1999) 1753–1758.
[39] A. Kusumi, Y. Sako, M. Yamamoto, Confined lateral diffusion of membrane receptors as studied by single particle tracking (nanovid microscopy). Effects of calcium-induced differentiation in cultured epithelial cells, Biophysical Journal 65 (1993) 2021–2040.
[40] S.M.L. Smith, Y. Lei, J. Liu, M.E. Cahill, G.M. Hagen, B.G. Barisas, D.A. Roess, Luteinizing hormone receptors translocate to plasma membrane microdomains following binding of human chorionic gonadotropin, Endocrinology 147 (2006) 1789–1795.
[41] E. Ortega, H. Schneider, I. Pecht, Possible interactions between the Fc epsilon receptor and a novel mast cell function-associated antigen, International Immunology 3 (1991) 333–342.

[42] A. Licht, J. Abramson, I. Pecht, Co-clustering activating and inhibitory receptors: impact at varying expression levels of the latter, Immunology Letters 104 (2006) 166–170.
[43] A. Licht, I. Pecht, R. Schweitzer-Stenner, Regulation of mast cells' secretory response by co-clustering the Type 1 Fcepsilon receptor with the mast cell function-associated antigen, European Journal of Immunology 35 (2005) 1621–1633.
[44] D. Holowka, J.A. Gosse, A.T. Hammond, X. Han, P. Sengupta, N.L. Smith, A. Wagenknecht-Wiesner, M. Wu, R.M. Young, B. Baird, Lipid segregation and IgE receptor signaling: a decade of progress, Biochimica et Biophysica Acta 1746 (2005) 252–259.